metals

MDPI

Article

Superficial Effects of Ball Burnishing on TRIP Steel AISI 301LN Sheets

Ramón Jerez-Mesa [1,*,†], Gemma Fargas [2], Joan Josep Roa [2], Jordi Llumà [2] and J. Antonio Travieso-Rodriguez [3]

1 Engineering Department, Faculty of Sciences and Technology, Universitat de Vic—Universitat Central de Catalunya, C. de la Laura 13, 08500 Vic, Spain
2 Materials Science and Engineering Department, Escola d'Enginyeria de Barcelona Est, Universitat Politècnica de Catalunya, Avinguda d'Eduard Maristany, 10-14, 08019 Barcelona, Spain; gemma.fargas@upc.edu (G.F.); joan.josep.roa@upc.edu (J.J.R.); jordi.lluma@upc.edu (J.L.)
3 Mechanical Engineering Department, Escola d'Enginyeria de Barcelona Est, Universitat Politècnica de Catalunya, Avinguda d'Eduard Maristany, 10-14, 08019 Barcelona, Spain; antonio.travieso@upc.edu
* Correspondence: ramon.jerez@uvic.cat; Tel.: +34-938-815-519
† Current address: Faculty of Sciences and Engineering, C. de la Laura 13, 08500 Vic, Spain.

Abstract: This paper explores the consequences of applying an ultrasonic vibration-assisted ball burnishing process and its non-vibration assisted version on the topology and subsurface microstructure of a transformation-induced plasticity AISI 301LN alloy. More specifically, four different metallographic conditions provided as 1.5-mm thickness sheets and characterized by different starting martensite content (3, 10, 20 and 40 wt.%) are included in the study. Ball burnishing was performed along the lamination direction and perpendicular to it. Results show that the effect of ball burnishing is strongly correlated with the pre-existing microstructure. The steel containing the lowest quantity of initial martensite is the most affected by the process, achieving a higher residual hardening effect, similar to the untreated steel with an original martensitic content of around 40 wt.%. Moreover, the process succeeds in generating a 100-nm thick nanograin layer under the plate subsurface. Finally, no conspicuous effect of the application of vibration assistance was observed, which encourages the application of alternative measurement techniques in future works to define its effect on the properties after being ball burnished.

Keywords: metastable austenitic stainless steel; TRIP effect; ball burnishing; acoustoplasticity; mechanical properties; phase transformation

check for updates

Citation: Jerez-Mesa, R.; Fargas, G.; Roa, J.J.; Llumà, J.; Travieso-Rodriguez, J.A. Superficial Effects of Ball Burnishing on TRIP Steel AISI 301LN Sheets. *Metals* **2021**, *11*, 82. https://doi.org/10.3390/met11010082

Received: 15 December 2020
Accepted: 30 December 2020
Published: 3 January 2021

Publisher's Note: MDPI stays neutral with regard to jurisdictional claims in published maps and institutional affiliations.

Copyright: © 2021 by the authors. Licensee MDPI, Basel, Switzerland. This article is an open access article distributed under the terms and conditions of the Creative Commons Attribution (CC BY) license (https://creativecommons.org/licenses/by/4.0/).

1. Introduction

Fuel economy and the reduction of greenhouse gas emissions have become a key factor for innovation in the automotive industry, given the restrictions imposed by the European Union after the environmental crisis. Indeed, it has been estimated that a 10% weight reduction in a vehicle can result in a 7% improvement of fuel economy and a 5% reduction of greenhouse gas emissions [1]. Therefore, the use of lighter materials with high strength properties has experienced a vast expansion during the last years. But besides low density-to-strength ratio, materials for the automotive industry must have a good formability to facilitate its processing and good energy absorption to guarantee passengers integrity in case of an accident. All these factors have lead car manufacturers to search for advanced materials and processes that can offer an enhanced service with a lowest weight and price of the final product.

In this context, advanced high strength steels are one of the most valued materials, especially multiphase steels with good ductility properties that can be maintained without compromising the required high strength. Specifically, metastable austenitic stainless steels are distinguished by their susceptibility to the Transformation Induced Plasticity (TRIP) effect whereby austenite (γ-phase) transforms into martensite (ε- and/or α'-) only by the

action of a deformation that has enough energy to induce a recrystallization change, even at ambient temperature [2]. That way, a superior strength-ductility balance can be obtained; exactly what is demanded by the automotive industry. These steels are one of the best candidates concerning crash behaviour properties, due to their high energy absorption potential, and are currently used to manufacture parts such as light train roofs and walls, chassis for buses or posts, frames and other carrying elements of the bodywork of private vehicles susceptible to being subjected to high impacts in accidents, for instance.

It has been reported in bibliography that a high resistance of components can be achieved to fulfil security requirements by modifying the material through volumetric controlled processes such as hydroforming [3]. However, typical failure modes associated to these alloys are usually originated on their surface, due to fatigue, fracture, wear and/or corrosion. Therefore, there is an utter interest to study and master the application of mechanical surface optimization treatments on this kind of alloys, such as sandblasting, shot peening or grinding, to promote grain nanostructuring or refinement on the subsurface to effectively enhance the global and in-service behaviour under real working conditions. Indeed, the high dependence of their properties on their manufacturing history makes it difficult to anticipate the actual condition of the TRIP alloys at the moment of their deployment. Hence the interest on controlling the traceability of the material before it is used for the manufacturing of final pieces, and the need to modify it through accurate and controlled manufacturing stages.

In this paper, ball burnishing (BB) is explored as a feasible process to superficially modify the material properties by induced microstructural changes while also fulfilling the traceability requirements that the material demands so that its properties can be mastered [4]. This is possible because of the way the process is planned and executed: through a numerical control routine that can be totally automated and integrated in the manufacturing roadmap of the target workpiece, and that achieves plastic deformation of the peaks of a surface texture by means of a ball that is moved over a target surface through adjacent passes [5]. BB is reported as having a triple comprehensive effect: roughness and texture reduction [6,7], hardness and compressive residual stresses increase of a surface layer nearly 0.5-mm deep [8], which can ultimately lead to an increase of fatigue lifespan [9]. These results reinforce the interest of exploring this process to modify metastable austenitic stainless steels because it could allow manufacturers to achieve a workpiece combining two different metallographic conditions with their respective mechanical performances, i.e., a part with hardened surface combined with a highly ductile core [10].

The idea of modifying TRIP steels surfaces through mechanical means has been previously explored by other authors through other surface modification techniques, such as electropulsing [11] or shot peening [12] to evaluate its effects on fatigue life [13,14] or wear resistance [15]. In later years, Fargas et al. (2015) [16] also proved the positive results of shot peening on fatigue life enhancement on metastable austenitic alloys, due to the fact that the process succeeded in completing martensitic transformation of the material on the surface. However, the authors also highlighted the fact that it had a detrimental effect on surface roughness, in fair agreement with similar works [17,18], because it is complicated to improve the finishing state of a laminated material.

This paper deals with the application of an ultrasonic vibration-assisted ball burnishing (UVABB) process on AISI 301LN sheets, one of the most commonly used stainless steel grades for light vehicles due to its excellent combination of formability and corrosion resistance. The success in applying UVABB is based on incorporating a piezoelectric resonant module on the BB tool that allows it to transmit a stable ultrasonic wave through the material lattice to change the way it is deformed by the ball [19]. Through this process, higher residual hardening can be achieved on deep layers of the surface [20], and it can prevent residual stress relaxation on materials such as Ti-6Al-4V alloys [21]. The main hypothesis explaining the positive effect of assisting the ball burnishing process with vibrations is based on the acoustoplastic effect, that is, a mechanism by which dislocations in a metal crystal lattice can travel further with the same level of stress, favouring subgrain

formation [22]. Li et al. (2016) [23] applied a different frequencies in a UVABB process to treat Ti-6Al-4V specimens, finding a higher concentration of surface dislocations as the frequency increases, and concluding that wear is enhanced to a highest extent if a 30-kHz assistance is performed. The effect could be improved by performing the process at temperatures around 120 [24].

During the last years, plenty of information related to the application of UVABB and thus superficially modify stainless steel alloys is available in the literature. Zhang et al. (2017) [25] achieved high compressive residual stress at 17-4 PH steel trough a 28-kHz assisted BB process. Liu et al. (2020) [26] have observed that an ultrasonic-assisted impact process can favour the nanocrystalization of 17-4 precipitation-hardening steels. Salmi et al. (2016) [27] achieved a 70.7% increase of residual hardness on 316L stainless steels specimens with a 20-kHz assisted process. Focusing on metastable austenitic stainless steels, which are the object of this contribution, Lesyk et al. (2019) [28] proved that UVABB delivered higher results in terms of surface integrity enhancement of AISI 304 surfaces with regards to other processes such as laser shock peening or water jet cavitation peening. Specimens of the same material evidence grain refinement when they are deformed with a 600-Hz pulsating force [29], that eventually leads to a higher expected fatigue life of cylindrical specimens [30]. Li et al. (2016) [31] applied an ultrasonic impact process, comparable to UVABB, to a SUS301 austenitic stainless steel, similar to the one object of study in this paper, and observed positive results in terms of surface roughness reduction, hardness improvement and subsequent higher resistance to wear.

Within this context and according to the explained background, the goal of this manuscript is to superficially modify and subsequently investigate the resulting microstructural (i.e., phase transformation, anisotropy, grain refinement, etc.) and mechanical properties of an AISI 301LN TRIP steel by means of UVABB. In fact, different TRIP steels with different degrees of accumulated cold work after pre-processing—hence with diverging metallographical conditions—will be included in the study and will be detailed in order to correlate the surface modification induced by the BB method as a function of the pre-martensitic content.

2. Experimental Procedure

2.1. Materials

The material used in order to conduct this research was a metastable austenitic stainless steel AISI 301LN provided by OCAS NV Arcelor-Mittal R&D Industry Gent (Belgium) as sheets of 1.5-mm thickness. The chemical composition of the steel expressed in elemental wt.% is: Fe-0.03C-17.36Cr-7.18Ni-1.68Mn-0.23Mo-0.55Si-0.14N. Four different materials were provided in different metallographic conditions, with different pre-existing martensitic content as well as different microstructural and mechanical properties as summarized in Table 1. Further information related to their microstructural properties for each investigated specimen can be found in Fargas et al. (2015) [32].

Table 1. Metallographical conditions of the AISI 301LN sheets included in the experimental procedure. After Fargas et al. (2015) [32].

State	% Martensite Mass Fraction	Grain Size (μm)	Yield Strength (MPa)	Tensile Strength (MPa)	Deformation at Break (%)	HV100
Annealed	<3%	11.70 ± 4.35	360 ± 6	902 ± 11	42 ± 2	240 ± 4
Cold worked	10%	8.55 ± 3.74	650 ± 7	967 ± 9	38 ± 6	300 ± 5
	20%	9.05 ± 4.21	926 ± 12	1113 ± 18	30 ± 5	400 ± 5
	40%	9.24 ± 4.19	1148 ± 17	1173 ± 20	21 ± 3	436± 7

2.2. Experimental Campaign

The UVABB process shall be executed by means of a prototype designed, manufactured, and characterized by Jerez-Mesa et al. (2018) [33]. It is equipped with a ball made of chrome

steel with 59 HRC hardness and 10 mm of diameter, which transmits the force during the process. Furthermore, a piezoelectric stack attached to the ball support allows for the ball burnishing operation to be assisted through a 40-kHz vibration when it is excited externally through a power circuit. The tool contains a calibrated compression spring whose function is to regulate the pre-charge force applied through the tool to the material, based on the length that it is compressed according to Hooke's law. That depth is controlled and kept constant during all tests through a numerical control code, which also contains the necessary interpolations to cover the whole target surface to be burnished.

Considering this kind of tool to perform the UVABB process, the experimental campaign is divided in two phases, as described below.

2.2.1. First Phase: Simple BB Tests

Preliminary experiments in this first phase have as an objective to analyse how the surfaces are affected by different BB pre-loads. With that aim, simple burnishing lines along and perpendicular to the lamination direction were performed in two different situations: when the piezoelectric is excited (UVABB) and when it is not (namely by applying non-vibration-assisted ball burnishing or NVABB). As shown in Table 2, five different levels of pre-load force are tested on all the investigated specimens with different pre-existing martensitic content in order to choose the best BB pre-load. Figure 1a shows the overall experimental setup. The burnishinng tool (2) is connected to an external power circuit (1) that excitates the piezoelectric stack inside to introduce the vibration assistance. In overall, 20 burnishing lines (4) where performed on each steel sheet (3) and then measured the residual depth in order to evaluate the deformation zone as a function of the burnishing force.

Table 2. Summary of the main testing parameters varied during the first experimental phase.

Factor	Levels/Description
Burnishing pre-load force (N)	100–200–300–400–500
Vibration assistance	VABB–NVABB
Burnishing direction with regards to lamination direction	perpendicular–parallel

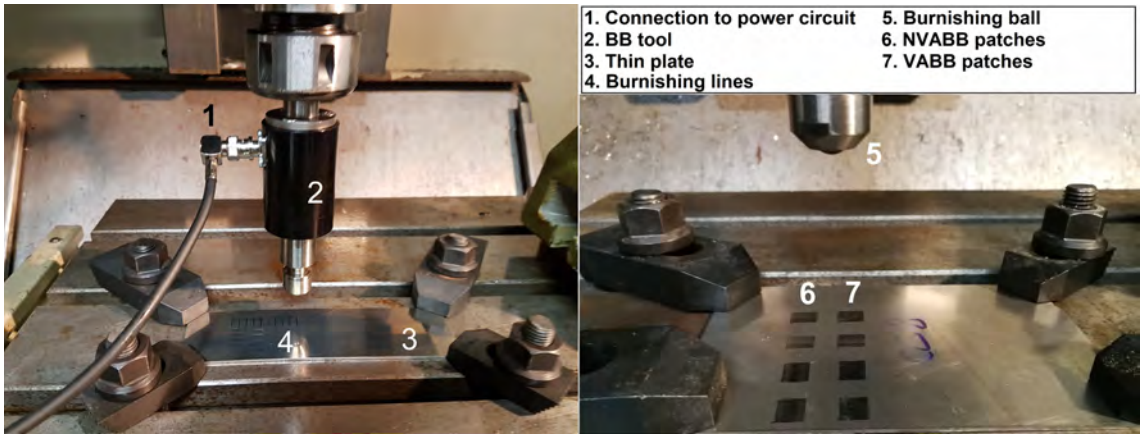

(**a**) (**b**)

Figure 1. (**a**) Experimental setup of the ultrasonic vibration-assisted ball burnishing (UVABB) experiment. (**b**) Eight patches performed on the plate with a 10 wt.% of pre-existing martensite during phase 2.

2.2.2. Second Phase: Simple BB Tests

During this phase, complete burnishing patches of 10 × 10 mm were performed on the different investigated surfaces. From the previous experimental application, the force is kept constant at 500 N for all the tested materials, whereas both directions of the space and both the UVABB and NVABB processes are considered. The number of passes is

introduced here as a new factor inside the experimental campaign (Table 3). The latter represents whether the burnishing patch is covered just once by adjacent passes separated 0.15 mm [34] to cover the whole patch, or five times. Consequently, for each material, 8 patches were performed on the surface as depicted in Figure 1b.

Table 3. Summary of the main testing parameters used during the second experimental phase.

Factor	Levels/Description
Vibration assistance	VABB–NVABB
Burnishing direction with regards to lamination direction	perpendicular–parallel
Number of passes	1–5

2.3. Characterization of BB Effects

2.3.1. Geometrical and Topological Features

Firstly, geometrical measurements were taken to know the dimensions of the lines performed during the first step. For the seconf phase of the experiments, the whole burnishing patches were analyzed in terms of topology. In both cases, the height distributions were acquired through a STIL MICROMESURE 2 (Aix-en-Provence, France) system equipped with a M-1R chromatic confocal sensor with a resolution of 10 nm. The dataset obtained from all measurements can be subsequently subjected to different roughness profile, texture and topological analysis with the SPIP software.

For the datasets obtained during the first phase, the basic geometrical descriptors of the burnishing profile through the transverse section were measured for all tested conditions in order to characterize the main plastic deformation features induced during the BB test, namely: width between pile-ups at the borders and height of the BB track, as depicted in Figure 2. The obtained values were then subjected to ANOVA calculations with the software Minitab 19 to evaluate the statistical significance of all factors considered in the experimental execution.

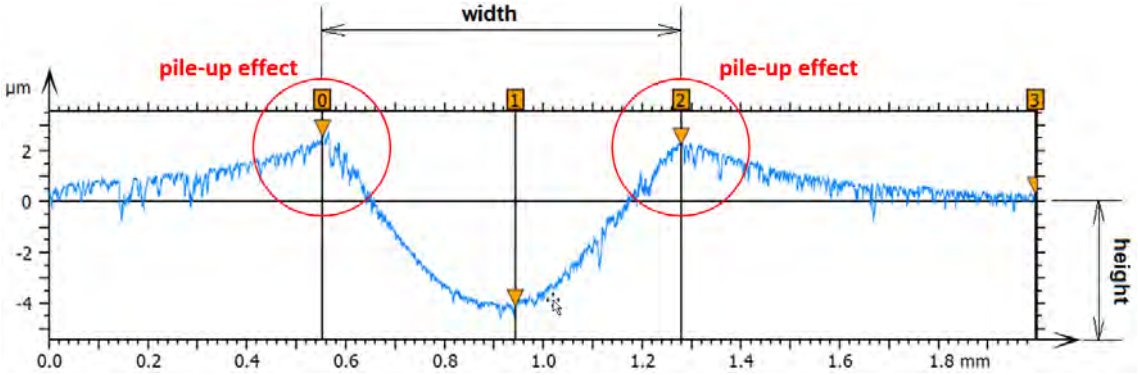

Figure 2. Cross-section profile performed on the monotonic residual track conducted at a maximum load of 400 N for the specimen with 10% of pre-existing martensite.

For the burnishing patches obtained during the second experimental step, the datasets acquired through the same equipment include the whole surface affected by the process. The average surface texture height (*Sa*, similar to the *Ra* parameter in 2D), is calculated on the target surface following the indications of the ISO 25178 standard [35]. In this case, in order to perform a surface damage analysis were also observed through a Phenom XL SEM (Thermofisher, Massachusetts, USA) at an acceleration voltage of 5 kV. This can help detecting possible failures such as flaking or microcracking provoked by the process, and to evaluate how ball burnishing affects the material which is directly visible.

2.3.2. Mechanical Characterization

Prior to the hardness measurements under the residual burnished track, the different specimens were sectioned by using a diamond wheel and subsequently embedded in Bakelite and mirror polished. Afterwards, hardness measurements were performed through Vickers indentation tests with a 0.5-kgf load by means of a Micromet 5114 hardness testing machine (Buehler, Germany). In order to correlate the microstructure and the mechanical properties induced during the BB effect, hardness tests profiles were built at different penetration depths, specifically at 20, 50, 80, 120, 175, 250, 400 and 600 μm. For each depth, five indentations were performed and averaged in order to get a statistical signification.

2.3.3. Microstructure Characterization and Damage by Contact Loading

Microstructural changes and deformation mechanisms induced during the BB process were characterized by micro-machining cross-sections below the surface by means of focused ion beam (FIB). Cross-sectioning and field emission scanning electron microscopy (FESEM) observations were conducted using a dual beam Workstation (Zeis Neon 40). A thin platinum layer was deposited on the region of interest prior to FIB with the main aim of reducing ion-beam damage. Then, a Ga+ ion source was employed to mill the surface at a voltage of 30 kV. A final polishing of the region of interest was performed at a current of 500 pA in order to get more details related to microstructural effects and the damage induced.

3. Results and Discussion

3.1. Geometrical Descriptors

3.1.1. Dimensions of BB Tracks (First Experimental Phase)

The width of burnishing lines and their depths were measured for all conditions described above. An analysis of variance (ANOVA) revealed that results are insensitive to vibration-assistance or to whether the lines were performed along the lamination direction or perpendicular to it (Figure 3). However, the increase of the force evidenced a higher value of both parameters, as could be expected assuming that if the effective area of contact of the ball with the surface has the same order of magnitude for all sheets, a higher force derives in higher mean contact pressure, hence provoking plastic deformation of the material to a further extent, which yields a larger track. Furthermore, the material also evidences that a higher pre-existing martensitic contents heterogeneously distributed inside the microstructure results in a lower line width, as a consequence of the higher hardness of the original material. Results make it very clear that the burnished geometry is strongly correlated with the pre-existing microstructure. On the other hand, one of the key parameters to take into consideration is the pile-up effect induced at the edges of the burnishing track as a symptom and consequence of self-hardening. In this sense, the track height results evidence that if the pre-existing martensite is higher or equal to 10%, it will experience a similar cold hardening rate. Rather, the sensitivity of the AISI 301LN alloy according to the pre-existing martensite% in terms of potential topological modification is high within the range 0–10%.

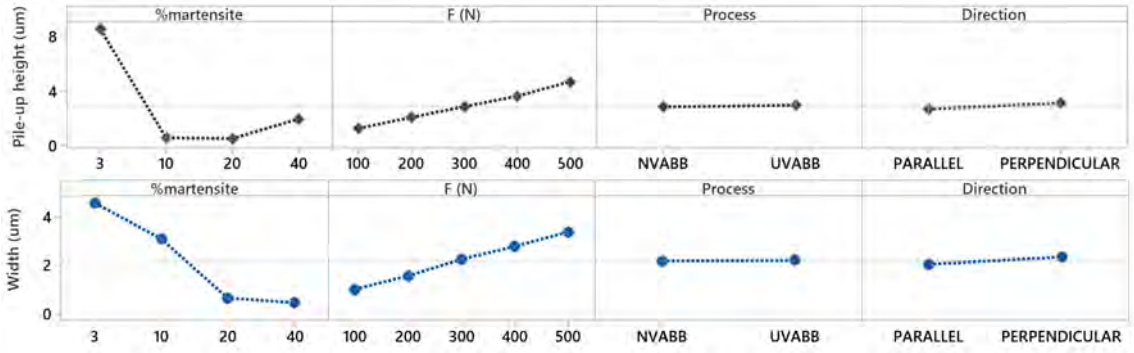

Figure 3. Mean effects of each factor on the imprint pile-up height (**top**) and width (**bottom**) executed through BB.

At sight of these results, it is decided that the experiments will be conducted at a 500-N constant pre-load. Moreover, these results evidence that the second stage of the experimental campaign is necessary because the burnished lines have proved their incapability of delivering conclusions about the influence of vibration assistance or the burnishing direction on the results.

3.1.2. Topology of BB Patches (Second Experimental Phase)

All specimens show an initial average texture amplitude *Sa* lower than 0.5 µm as a consequence of the lamination process from which they come from. As it is an extremely low value, the application of BB results in an increase of *Sa* and all surface features are strongly oriented along the burnishing direction. Therefore, results are independent of the burnishing direction, and for this reason only those obtained in the transverse direction are shown in this section. Much on the contrary, a different effect of the process can be observed depending on whether the material has a higher pre-existing weight fraction of martensite, as shows Figure 4. A single pass on the specimen with a 3% of pre-existing martensite results in the highest increase of *Sa*, which was to be expected at sight of the results obtained in the previous subsection. However, it is interesting to notice that in this case, ulterior passes of BB succeed in reducing those peaks again, meaning that the higher affectation of this metallographic condition can also work in favour of topology improvement. This is true for both the assisted process and the non-assisted. On the other hand, surfaces with 10% or more of pre-existing martensite experience an increase of *Sa*, that is deteriorated with further passes. This can be associated to the fact that these specimens experience less pile-up effect and less self-hardening. The cyclic effect of BB, through which a surface is improved to a certain extent, but harmed if further plastic deformation is performed, has been already observed previously [20]. Therefore, this result evidences again that the original microstructure of the material is relevant to define the ulterior effects of ball burnishing.

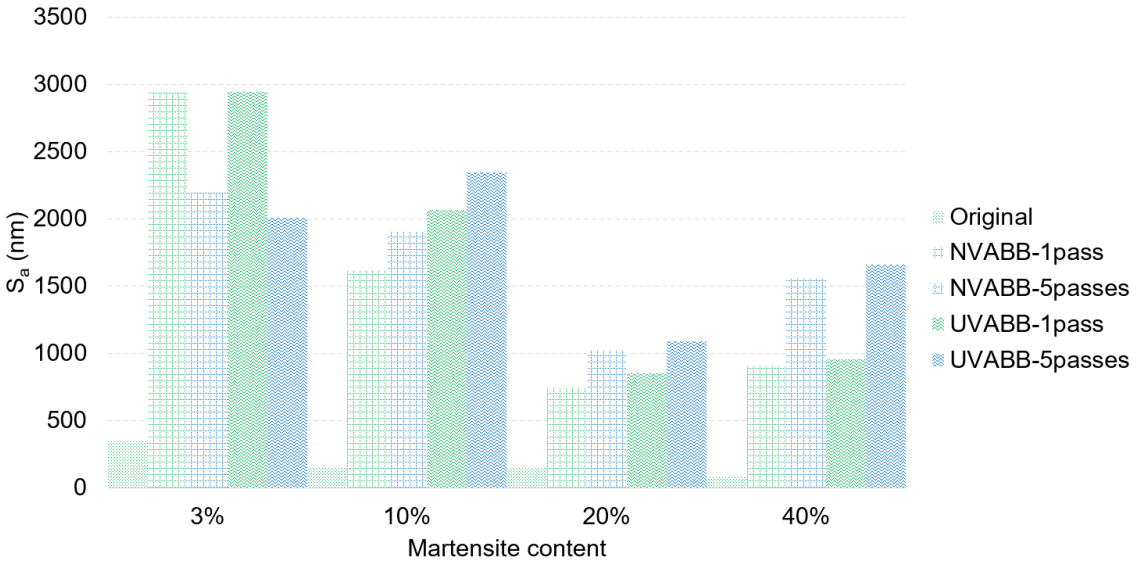

Figure 4. Average surface texture amplitude for the tested specimens burnished in the transverse direction.

The comparison of the UVABB and NVABB evidences that after the assisted process, the specimens present higher *Sa* values. It can be explained by the fact that the acoustoplastic effect caused by the vibration assistance results in higher plastic deformation. As an example, visual inspection (Figure 5) shows that the topology of the material with 10% of pre-existing martensite presents higher peaks when treated through the vibration-assisted process.

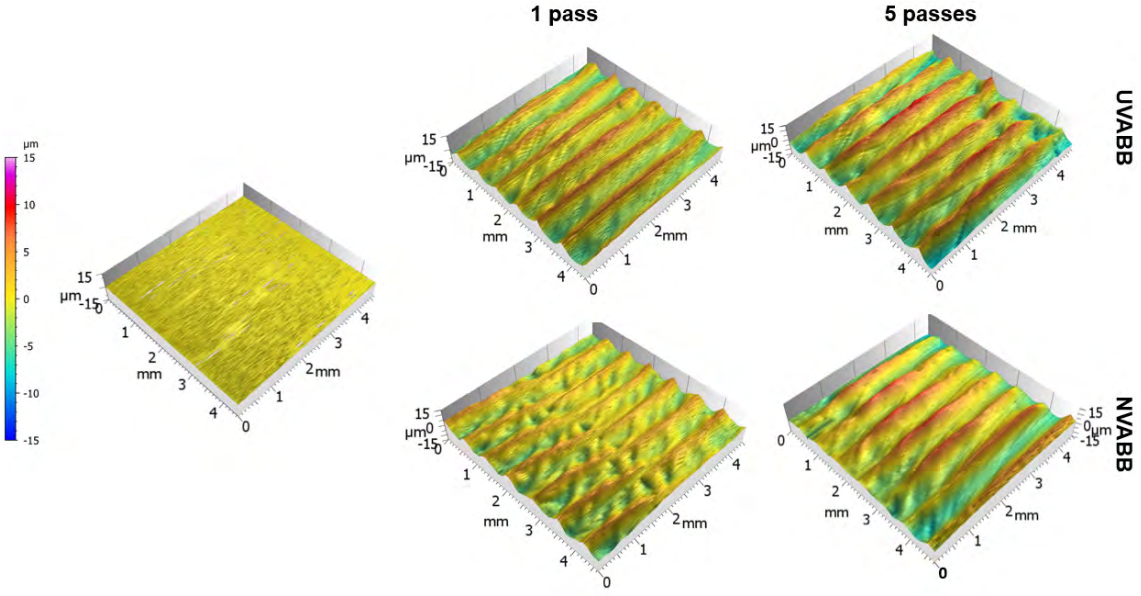

Figure 5. Three-dimensional reconstruction of the surface texture modification of material with 10% pre-existing martensite burnished along the transverse direction.

Previous results show that texture improvement of AISI 301LN laminated sheets through UVABB cannot be justified because it results on a rougher surface. The non-vibration assisted process should be advised fron this perspective. To complete the analysis through visual inspection, SEM micrographs can be consulted (Figure 6). The direction of the BB process defines the directionality of the new surface features. Moreover, the peaks generated after the process are conspicuous, although more acute in the case of the material with less amount of the pre-existing martensitic phase. Remarkable surface damage (like cracks, pores, etc.) are observed as craters and dragged material on the specimen with a lower pre-existing martensite content. Ductility proves to go against a positive result of ball burnishing on AISI 301LN plates, as it drives the process into severe plastic deformation and crater formation, which results in potential crack nucleation focuses.

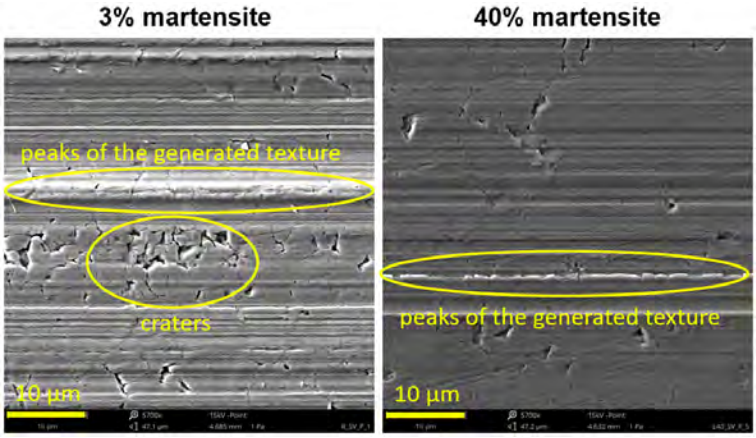

Figure 6. SEM micrographs showing the main details of UVABB surfaces.

3.2. Deep Hardness Profiles

The analysis of all hardness profiles conducted at the micrometric length scale after VABB and NVABB has revealed that the effect of vibration assistance is not relevant either from this perspective. For that reason, Figure 7 only shows the deep hardness profile of the surface after UVABB. Moreover, the higher content of martensite in the initial structure reduces the penetration of the effect of the residual hardening effect of both processes in both cases. The thickness of the affected layer is higher for the specimen with an initial 3%

martensitic content and is lower as that value increases. Furthermore, when the amount of the pre-existing martensite is higher than 20%, the deformed layer remains stable. In relative improvement terms, an increase of 60.3% 156HV50 hardness is detected in the 3% specimen, whereas this value is around 9.5% for the specimens with higher content of martensite. The amount of initial martensite is therefore one of the key parameters to define the expected residual hardness improvement of the material near the zone affected by the BB process. On the other hand, these profiles show similar behaviour in both directions, and therefore, it cannot be stated that the relative direction of ball burnishing with regards to the original lamination direction is influential in these terms.

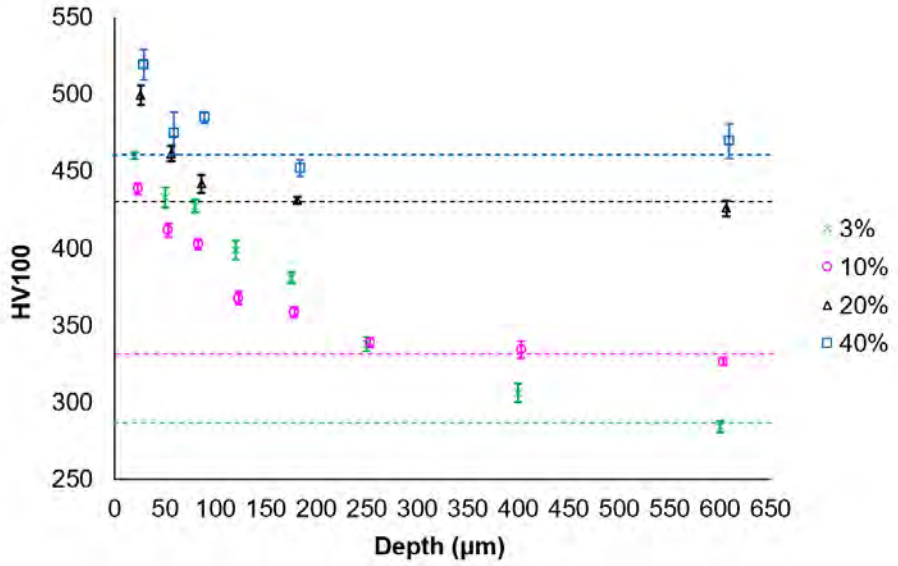

Figure 7. Deep hardness profiles for the UVABB tests in the parallel direction as a function of the initial martensite content. Discontinuous lines: core material hardness.

3.3. Microstructural Characterization

The examination of the deformed subsurface microstructure is essential to reach a proper understanding of the change in surface properties that occurs during the BB process. Figure 8 exhibits a FESEM micrograph of a cross-section performed at the central part of the BB track. This area corresponds to the region where the burnishing ball was pressed at the maximum load against the surface of the specimen and the high generated contact stress field was able to induce a very thin surface layer of new nano-grains of about 20–30 nm in diameter with a nanolayer thickness of around 100 nm (marked with a dashed white line and labelled as (1) in Figure 8), which may be formed by in-situ recrystallization from the highly deformed AISI 301 LN surface. Due to the high strain induced during the burnishing process, progressive misorientation of dislocation cells lead to the formation of new nano-sized grains, in fair agreement with Minguela et al. (2020) [36] for zirconia based ceramic materials superficially modified by grinding process. Furthermore, immediately below this initial nanograin layer the AISI 301LN, grains are slightly rotated due to shear stress generated by the feed movement of the burnishing ball on the surface. This is labelled as (2) in the FESEM micrograph. Indeed, the induced stress at that depth is less severe than on the immediate surface. It is worth mentioning that it is possible to induce phase transformation from $\gamma \rightarrow \varepsilon$ and/or α'-martensite during this deformation process and that it is one of the main hardening mechanisms induced during the BB process, but this deformation phenomenon is out from the scope of this manuscript and is to be considered for future works.

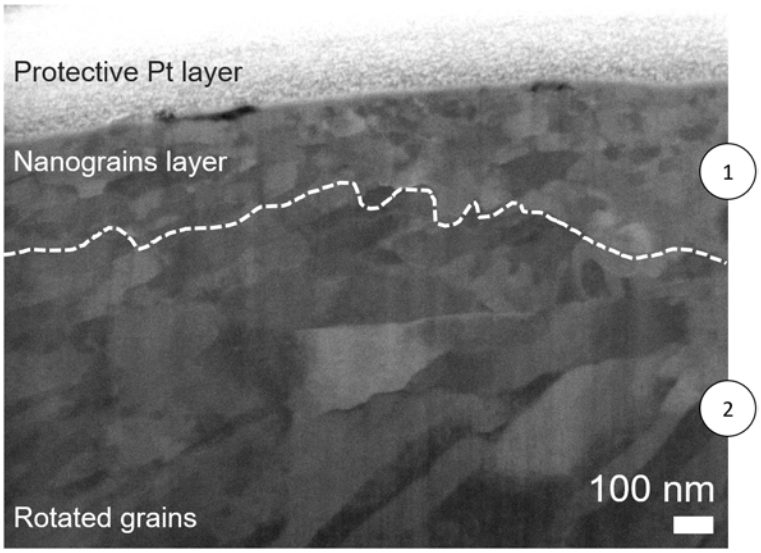

Figure 8. Nanograins layer observed on the subsurface of the specimen with initial contents of 40% martensite and processed through UVABB.

4. Conclusions

The results shown in this contribution have demonstrated that the effects of ball burnishing on laminated AISI 301LN surfaces are highly dependent on the as-received microstructure. The higher the contents of martensite, less conspicuous are the effects of the process both in terms of surface texture generation and residual deep hardening of the material. Indeed, the annealed AISI 301LN condition (i.e., with an original contents of 3% of martensite) has evidenced the highest affectation after being subjected to the ball burnishing process, which succeeds in achieving the deepest effect of residual hardening down to a 250-μm depth. The hardness of the immediate surface was increased in almost 65% with regards to the core material. SEM observations also pointed out the formation of a thin nanograin layer as a consequence of the severe plastic deformation introduced by the applied mechanical process.

The application of vibration assistance has not delivered an enhancement on the process itself and can even show worse results in terms of the generated texture. However, it is important to highlight that these results have been tested on laminated specimens, which depart from an excellent surface topology, and could change if the process was applied on other kind of surfaces finished through chip removal such as ball end milling, which defines part of the future works to be conducted on this issue. Moreover, the comprehensive analysis showed in this paper proves that the results observed at the microscopical level are insufficient to define the effect of ball burnishing on the AISI 301LN steel. Therefore, advanced techniques are required to achieve a better understanding of the effects of the process on this kind of material. In future steps, in situ techniques shall be applied to measure residual stress and microstructural change that could lead to a further knowledge of the process itself.

Author Contributions: conceptualization, R.J.-M. and G.F.; methodology, R.J.-M., J.J.R. and G.F.; software, G.F.; validation, J.A.T.-R.; formal analysis, R.J.-M., J.J.R. and G.F.; investigation, R.J.-M., J.J.R. and G.F.; resources, R.J.-M., G.F., J.J.R., J.L. and J.A.T.-R.; data curation, R.J.-M., G.F., J.J.R., J.L. and J.A.T.-R.; writing–original draft preparation, R.J.-M., J.L. and J.A.T.-R.; writing–review and editing, R.J.-M., G.F., J.J.R., J.L. and J.A.T.-R.; visualization, R.J.-M., G.F., J.J.R., J.L. and J.A.T.-R.; supervision, R.J.-M.; project administration, G.F.; funding acquisition, R.J.-M. and G.F. All authors have read and agreed to the published version of the manuscript.

Funding: Financial support for this study was provided by the Ministry of Science, Innovation and Universities of Spain, through grant RTI2018-101653-B-I00, which is greatly appreciated. Also by

the regional government of Catalonia and FEDER funds for regional development through grant IU68-016744.

Institutional Review Board Statement: Not applicable.

Informed Consent Statement: Not applicable.

Data Availability Statement: Not applicable.

Acknowledgments: J.J. Roa acknowledges the Serra Hunter program of the Generalitat de Catalunya.

Conflicts of Interest: The authors declare no conflict of interest.

Abbreviations

The following abbreviations are used in this manuscript:

BB	Multidisciplinary Digital Publishing Institute
FESEM	Field Emission Scanning Electron Microscopy
NVABB	Directory of open access journals
SEM	Scanning Electron Microscopy
VABB	Three letter acronym

References

1. Ghassemieh, E. Materials in automotive application, state of the art and prospects. In *New Trends and Developments in Automotive Industry*; InTech: New York, NY, USA, 2011; pp. 365–394.
2. Krupp, U.; West, C.; Christ, H.J. Deformation-induced martensite formation during cyclic deformation of metastable austenitic steel: Influence of temperature and carbon content. *Mater. Sci. Eng. A* **2008**, *481*, 713–717. [CrossRef]
3. Mangonon, P.L.; Thomas, G. The martensite phases in 304 stainless steel. *Metall. Trans.* **1970**, *1*, 1577–1586. [CrossRef]
4. Robles, A.S.; De la Peña, J.Á.D.; García, A.d.J.B.; Gómez, E.A.; MORA, H.P.; Robles, N.S. El proceso de bruñido con bola: Estado del arte de una tecnología en desarrollo. *DYNA* **2017**, *92*, 28–33. [CrossRef]
5. Sachin, B.; Narendranath, S.; Chakradhar, D. Selection of optimal process parameters in sustainable diamond burnishing of 17-4 PH stainless steel. *J. Braz. Soc. Mech. Sci. Eng.* **2019**, *41*, 219. [CrossRef]
6. Rotella, G.; Rinaldi, S.; Filice, L. Roller burnishing of Ti6Al4V under different cooling/lubrication conditions and tool design: effects on surface integrity. *Int. J. Adv. Manuf. Technol.* **2020**, *106*, 431–440. [CrossRef]
7. Ding, Z.; Zhao, J.; Liu, H.; Dong, Y. Effects of ball burnishing on surface properties of SKD11 mold steel. *Eng. Res. Express* **2020**, *2*, 025004. [CrossRef]
8. Hamadache, H.; Bourebia, M.; Taamallah, O.; Laouar, L. Surface hardening of 36 NiCrMo 6 steel by ball burnishing process. *Mater. Res. Express* **2019**, *6*, 106538. [CrossRef]
9. Travieso-Rodríguez, J.A.; Jerez-Mesa, R.; Gómez-Gras, G.; Llumà-Fuentes, J.; Casadesús-Farràs, O.; Madueño-Guerrero, M. Hardening effect and fatigue behavior enhancement through ball burnishing on AISI 1038. *J. Mater. Res. Technol.* **2019**, *8*, 5639–5646. [CrossRef]
10. Kuznetsov, V.; Smolin, I.Y.; Dmitriev, A.; Tarasov, S.Y.; Gorgots, V. Toward control of subsurface strain accumulation in nanostructuring burnishing on thermostrengthened steel. *Surf. Coat. Technol.* **2016**, *285*, 171–178. [CrossRef]
11. Wang, S.; Li, Y.; Yao, M.; Wang, R. Compressive residual stress introduced by shot peening. *J. Mater. Process. Technol.* **1998**, *73*, 64–73. [CrossRef]
12. Terres, M.A.; Laalai, N.; Sidhom, H. Effect of nitriding and shot-peening on the fatigue behavior of 42CrMo4 steel: Experimental analysis and predictive approach. *Mater. Des.* **2012**, *35*, 741–748. [CrossRef]
13. Nikitin, I.; Altenberger, I. Comparison of the fatigue behavior and residual stress stability of laser-shock peened and deep rolled austenitic stainless steel AISI 304 in the temperature range 25–600 C. *Mater. Sci. Eng. A* **2007**, *465*, 176–182. [CrossRef]
14. Torres, M.; Voorwald, H. An evaluation of shot peening, residual stress and stress relaxation on the fatigue life of AISI 4340 steel. *Int. J. Fatigue* **2002**, *24*, 877–886. [CrossRef]
15. Palacios, M.; Bagherifard, S.; Guagliano, M.; Fernández Pariente, I. Influence of severe shot peening on wear behaviour of an aluminium alloy. *Fatigue Fract. Eng. Mater. Struct.* **2014**, *37*, 821–829. [CrossRef]
16. Fargas, G.; Roa, J.; Mateo, A. Effect of shot peening on metastable austenitic stainless steels. *Mater. Sci. Eng. A* **2015**, *641*, 290–296. [CrossRef]
17. De Los Rios, E.; Trull, M.; Levers, A. Modelling fatigue crack growth in shot-peened components of Al 2024-T351. *Fatigue Fract. Eng. Mater. Struct.* **2000**, *23*, 709–716. [CrossRef]
18. Guagliano, M.; Vergani, L. An approach for prediction of fatigue strength of shot peened components. *Eng. Fract. Mech.* **2004**, *71*, 501–512. [CrossRef]
19. Estevez-Urra, A.; Llumà, J.; Jerez-Mesa, R.; Travieso-Rodriguez, J.A. Monitoring of Processing Conditions of an Ultrasonic Vibration-Assisted Ball-Burnishing Process. *Sensors* **2020**, *20*, 2562. [CrossRef]

20. Jerez-Mesa, R.; Landon, Y.; Travieso-Rodriguez, J.A.; Dessein, G.; Lluma-Fuentes, J.; Wagner, V. Topological surface integrity modification of AISI 1038 alloy after vibration-assisted ball burnishing. *Surf. Coat. Technol.* **2018**, *349*, 364–377. [CrossRef]
21. Jerez-Mesa, R.; Travieso-Rodríguez, J.A.; Landon, Y.; Dessein, G.; Lluma-Fuentes, J.; Wagner, V. Comprehensive analysis of surface integrity modification of ball-end milled Ti-6Al-4V surfaces through vibration-assisted ball burnishing. *J. Mater. Process. Technol.* **2019**, *267*, 230–240. [CrossRef]
22. Siu, K.; Ngan, A.; Jones, I. New insight on acoustoplasticity–ultrasonic irradiation enhances subgrain formation during deformation. *Int. J. Plast.* **2011**, *27*, 788–800. [CrossRef]
23. Li, G.; Qu, S.; Pan, Y.; Li, X. Effects of the different frequencies and loads of ultrasonic surface rolling on surface mechanical properties and fretting wear resistance of HIP Ti–6Al–4V alloy. *Appl. Surf. Sci.* **2016**, *389*, 324–334. [CrossRef]
24. Li, G.; Qu, S.; Xie, M.; Li, X. Effect of ultrasonic surface rolling at low temperatures on surface layer microstructure and properties of HIP Ti-6Al-4V alloy. *Surf. Coat. Technol.* **2017**, *316*, 75–84. [CrossRef]
25. Zhang, Q.; Hu, Z.; Su, W.; Zhou, H.; Liu, C.; Yang, Y.; Qi, X. Microstructure and surface properties of 17-4PH stainless steel by ultrasonic surface rolling technology. *Surf. Coat. Technol.* **2017**, *321*, 64–73. [CrossRef]
26. Liu, D.; Liu, D.; Zhang, X.; Ma, A.; Liu, C. Microstructural evolution mechanisms in rolled 17-4PH steel processed by ultrasonic surface rolling process. *Mater. Sci. Eng. A* **2020**, *773*, 138720. [CrossRef]
27. Salmi, M.; Huuki, J.; Ituarte, I.F. The ultrasonic burnishing of cobalt-chrome and stainless steel surface made by additive manufacturing. *Prog. Addit. Manuf.* **2017**, *2*, 31–41. [CrossRef]
28. Lesyk, D.; Soyama, H.; Mordyuk, B.; Dzhemelinskyi, V.; Martinez, S.; Khripta, N.; Lamikiz, A. Mechanical surface treatments of AISI 304 stainless steel: Effects on surface microrelief, residual stress, and microstructure. *J. Mater. Eng. Perform.* **2019**, *28*, 5307–5322. [CrossRef]
29. Wang, H.; Song, G.; Tang, G. Effect of electropulsing on surface mechanical properties and microstructure of AISI 304 stainless steel during ultrasonic surface rolling process. *Mater. Sci. Eng. A* **2016**, *662*, 456–467. [CrossRef]
30. Wang, H.b.; Yang, X.h.; Li, H.; Song, G.l.; Tang, G.y. Enhanced fatigue performance and surface mechanical properties of AISI 304 stainless steel induced by electropulsing-assisted ultrasonic surface rolling process. *J. Mater. Res.* **2018**, *33*, 3827–3840. [CrossRef]
31. Li, L.; Kim, M.; Lee, S.; Bae, M.; Lee, D. Influence of multiple ultrasonic impact treatments on surface roughness and wear performance of SUS301 steel. *Surf. Coat. Technol.* **2016**, *307*, 517–524. [CrossRef]
32. Fargas, G.; Zapata, A.; Roa, J.J.; Sapezanskaia, I.; Mateo, A. Correlation between microstructure and mechanical properties before and after reversion of metastable austenitic stainless steels. *Metall. Mater. Trans. A* **2015**, *46*, 5697–5707. [CrossRef]
33. Jerez-Mesa, R.; Travieso-Rodriguez, J.A.; Gomez-Gras, G.; Lluma-Fuentes, J. Development, characterization and test of an ultrasonic vibration-assisted ball burnishing tool. *J. Mater. Process. Technol.* **2018**, *257*, 203–212. [CrossRef]
34. Gomez-Gras, G.; Travieso-Rodriguez, J.A.; Jerez-Mesa, R.; Lluma-Fuentes, J.; de la Calle, B.G. Experimental study of lateral pass width in conventional and vibrations-assisted ball burnishing. *Int. J. Adv. Manuf. Technol.* **2016**, *87*, 363–371. [CrossRef]
35. Dong, W.; Sullivan, P.; Stout, K. Comprehensive study of parameters for characterising three-dimensional surface topography: III: Parameters for characterising amplitude and some functional properties. *Wear* **1994**, *178*, 29–43. [CrossRef]
36. Minguela, J.; Slawik, S.; Mücklich, F.; Ginebra, M.; Llanes, L.; Mas-Moruno, C.; Roa, J. Evolution of microstructure and residual stresses in gradually ground/polished 3Y-TZP. *J. Eur. Ceram. Soc.* **2020**, *40*, 1582–1591. [CrossRef]